Sandia Laboratories

Albuquerque, New Mexico 87115
4441/ML-15
September 29, 1980

Mr. Richard Sherry
U. S. Nuclear Regulatory Commission
Fuel Behavior Research Branch
Division of Reactor Safety Research
MS1130-SS
Washington, DC 20555

Dear Rick:

Enclosed are the status reports for the month August for the core melt and separate effects programs.

Sincerely,

Marshall

M. Berman, Supervisor
Reactor Safety Studies
Division 4441

I. Steam Explosion

We continued this month to check out the small scale high ambient pressure chamber. New viewing ports of zinc silicate are being ordered for the high pressure tests. In the interim, atmospheric tests using $FeO_{1.3}$ in air are being conducted in the new chamber to assure that the experimental technique will be successful and that the experimental behavior will not change. Two tests have been successfully performed and the results are similar to what was observed outside the chamber. In addition, experiments using $FeO_{1.1-1.3}$ in argon are being performed. The ambient oxygen partial pressure can be varied to change the iron-oxide composition. These tests will examine the effect of oxygen content on the explosion efficiency.

During the past month the FITS delivery system was modified to improve the delivery process. An additional EXO-FITS experiment (MD-19) was conducted to verify that the modifications were adequate. The delivery system was also successfully tested at 1.04 MPa in the FITS chamber.

FITS5A will be conducted during the first week in September and will have the same initial conditions as FITS4A (1.04 MPa chamber pressure, 5.5 kg of Fe-Al_2O_3 melt). The purpose of FITS5A is to:

1) Demonstrate the high pressure capability of the FITS system.
2) Observe the effect of high ambient pressure on explosivity.
3) Supply an external trigger source late in time if no spontaneous explosion occurs.

Data from earlier experiments (MD series) were used to set the external trigger firing time. Spontaneous explosions normally occurred 0.1 to 0.2 sec after melt entry into the water; the trigger will fire 0.4 sec after melt entry.

Data from pressure transducers in the recent experiments (e.g. MD-19) have normally indicated peak explosion pressures on the order of hundreds of bars. However, some previously measured pressures much greater than 1000 bars are now believed to have been caused by spurious electrical breakdown on the lithium-niobate gage. A detonation theory calculation (Chapman-Jouget pressures) indicates that the explosion pressures should be in the range of 100 - 500 bars.

The preliminary results of test MD-19 are the following:

Melt Mass	5.1 kg delivered
Water Mass	224 kg
Water Temp.	25.5°C
Entry Velocity	5.74 m/s
Time from entry to explosion	0.176 sec.
Propagation Velocity	427 m/s
Peak explosion pressure	10 MPa

The two topical reports on explosion modelling and containment failure probability were finished this month and are now being typed and reviewed. Informal first drafts should be available by the end of September

II. Core-Concrete Interactions

CORCON development, application and documentation activities continued during August. An inconsistency was found in the way in which the enthalpy of concrete was being calculated (in CORCON-MOD0) as the concrete is heated from its initial or virgin condition to the temperature of the molten pool. The code contains fits to curves of enthalpy versus temperature for each of the three default concretes. These curve fits were used to evaluate the change in concrete enthalpy as the virgin concrete was heated to its ablation temperature. The change in enthalpy of condensed concrete ablation products from ablation temperature to pool temperature, however, is calculated using subroutine CPENTH. These two procedures were not consistent with the result that the total energy necessary to raise virgin concrete to the pool temperature was a

function of the ablation temperature. To rectify this, the curve fits have been replaced by an internal enthalpy c 'culation that duplicates the one used to generate the original curves but uses the data base embodied in CPENTH and CONFND. In addition to being consistent, the new procedure simplifies the imput needed for a non-standard concrete in that the concrete heat of ablation is no longer required.

As part of the continuing effort to properly model the freezing behavior of the melt, efforts were directed toward improving the models used for determining the solidus and liquidus temperatures of the metallic and oxidic phases. In CORCON-MODO, this is done in subroutine SOLLIQ which was taken virtually unchanged from the INTER code (as a first approximation), but is really inadequate for the phase compositions employed in CORCON. An improved model has been developed for the metallic phase which is based on the assumption that the bulk of this phase will be stainless steel. It consists of a simple fit for the solidus-liquidus surfaces for the Fe-Ni-Cr ternary system. Consideration is being given to using a similar approach for the oxidic phase by treating it as a ternary system of concrete oxides, metallic oxides and fuel oxides. Some conceptual progress has been made, but it is clear that the oxidic system is substantially more complicated.

As mentioned last month, calculations for the code comparison test conditions have indicated: 1) that the melt temperature history is quite sensitive to the heat transfer between pool layers

and from the pool surface, and 2) that the Blottner heat transfer correlations yield coefficients substantially higher than anticipated. The latter could be attributed either to the inability of the correlations to model the physical phenomena involved (due to incorrect formulations or application outside their range of applicability) or to the use of incorrect values of the material properties appearing in the correlations. The latter was explored by investigating the changes induced in the transport properties by partial freezing of the melt (i.e., by the precipitation of solids). A pronounced effect occurs in the viscosity which increases significantly as the volume fraction of solids increases. As a simple first attempt at including this effect, we have replaced the viscosity in the correlations by the two-phase viscosity, using the Kunitz two-phase multiplier to account for suspended solids. Further, we are currently evaluating this factor at the interface temperature (rather than at the layer bulk temperature) in order to better represent conditions in the boundary layer. Further work in this area is clearly needed. We are not entirely happy with the changes described above and feel that improvement of the heat transfer correlations should have a high priority in future CORCON development activities.

Development of a decay heat generation model for inclusion in CORCON was completed during August. The model calculates the internal heat generation in a core melt during a melt/concrete interaction due to the nuclear decay of radioactive elements in the melt. It includes three considerations: elemental power generation; melt loss during core meltdown, leading to a melt

composition at the onset of the melt/concrete interaction; and material loss during the interaction due to vaporization and mechanical sparging (i.e., aerosol generation). Coding of the model is underway.

Additional activities included CORCON, INTER, and WECHSL calculations for the code comparison test conditions (no results of note) and, modifications to the CORCON input/output sections and plot routines. Preparation of a CORCON topical-report/users-manual continued.

III. Separate Effects Tests for TRAP Code Development

The purpose of the separate effects tests is to identify the vapor species existing in steam environments which contain fission-product elements and to measure the required physical properties of these species.

Transpiration Experiments: We have completed a quantitative analysis of the data from the CsOH transpiration experiments. Forming gas (98% N_2 + 2% H_2) was used as a carrier gas. These experiments have allowed us to determine the vapor pressure of CsOH over the temperature range 520-720°C. Data are plotted in Figure 1 as a function of 1/T. Except for the two lowest temperatures (largest values of 1/T) cases, the data are well represented by the expression

$$\text{Log } P = 8.46 - 7306/T$$

where P is the vapor pressure of CsOH in torr and T is the temperature in K. The two lowest temperature cases were run over

weekends without being monitored. Since the above expression is not within the generous error bars of these two data points, we will repeat these cases with closer monitoring.

Figure 1 also shows the CsI vapor pressure curve previously measured by us and others. Note that the vapor pressure for CsOH is about a factor of 20 larger than that for CsI at the same temperature. This result is somewhat unexpected since the vapor pressures of sodium and potassium compounds (hydroxides and iodides) are much more similar.

Tellurium Experiments: Last month we reported a tentative value for the rate of desorption of tellurium from nickel-tellurium solid solutions. The rate is linear and over the temperature range 800-980°C. It is represented by the expression

$$\log k = 4.61 - 9500/T$$

where k is measured in mg Te/cm^2/min and T is the temperature in K. During August we confirmed the validity of this rate expression using flowrates of oxygen carrier gas that were higher (100 scc/min) and lower (25 scc/min) than that used during July (50 scc/min). Since the above expression remained valid over a range of gas velocities, we conclude that the rate is characteristic of the desorption process and not of the gas transport process. During July we concluded that, since the rate was linear, it did not represent the internal diffusion process. The net result of our work during July and August is the conclusion that the expression given above does represent the rate of removal of tellurium gas from the near-surface region.

Additional experiments are being performed to determine the effect of water vapor on the desorption rate of tellurium from Ni-Te solid solutions.

Interim Laser System: During the month of August we began our first series of hot tests in the interim system. We used the Raman Spectroscopy setup to examine Raman scattering from N_2, H_2O, and H_2 inside the cell at room and elevated temperatures. A copy of the actual data from two H_2 experiments is shown in Figure 2. Pure rotational Raman spectra of H_2 are shown in this figure at room and elevated temperatures. The rotational temperatures indicated in Figure 2 were determined graphically using the measured rotational line intensities. A Boltzmann plot of the normalized line intensities versus the rotational term value, $F_o(J)$ is shown in Figure 3. The rotational temperatures are calculated using the slopes of the lines that pass through the data.

As indicated in our previous monthly report, the Raman spectroscopy setup that we are presently using will be returned to its owners in October. We are negotiating for the purchase of a similar setup, but we still anticipate some decrease in our Raman spectroscopy effort during October and possibly November.

Fission Product Reaction Facility (FPRF): The purpose of the FPRF is to aid in the study of the chemistry resulting from the reaction of single or multiple fission-product vapors with steam and with the containing vessel at high temperatures and for long residence times. The operating characteristics provide for residence times up to several hours, system temperatures up to

1000°C, and fission-product concentrations of ~10^{-3} g/cm^3. Reaction products will be examined by Raman Spectroscopy, analysis of condensate on sample coupons, and analysis of samples collected from the steam. At this time the status of the FPRF is as follows:

Conceptual design	-	100% complete
Detailed design	-	100% complete
Fabrication	-	90% complete
Assembly	-	30% complete
Proof testing	-	20% complete

Copy to:
NRC Public Document Room (2)
R. A. Bari, BNL
I. Catton, U of C, NEL
Dae Cho, ANL
M. Cunningham, NRC, RES
R. Denning, BCL
R. DiSalvo, NRC, RES
J. Gieseke, BCL
M. W. Johnston, NRC, RES
D. Hoatson, NRC, RES
J. Long, NRC, NRR
T. Malinauskas, ORNL
A. Marchese, NRC, NRR
J. Meyer, NRC, NRR
W. Milstead, NRC, NRR
J. Murphy, NRC, RES
J. Norberg, NRC, OSD
W. Pasedag, NRC, NRR
G. Quittschreiber, NRC, ACRS
J. Read, NRC, NRR
M. Silberberg, NRC, RES
T. Speis, NRC, NRR
D. Swanson
T. Walker, NRC, RES
R. Wright, NRC, RES
2514 - D. E. Mitchell
4400 - A. W. Snyder
4422 - R. M. Elrick
4422 - D. A. Powers
4440 - G. R. Otey
4441 - R. K. Cole
4441 - M. L. Corradini
4441 - J. C. Cummings
4441 - J. F. Muir
4442 - W. A. VonRiesemann
5836 - L. S. Nelson
5836 - R. A. Sallach
4441 - M. Berman
3151 - W. L. Garner

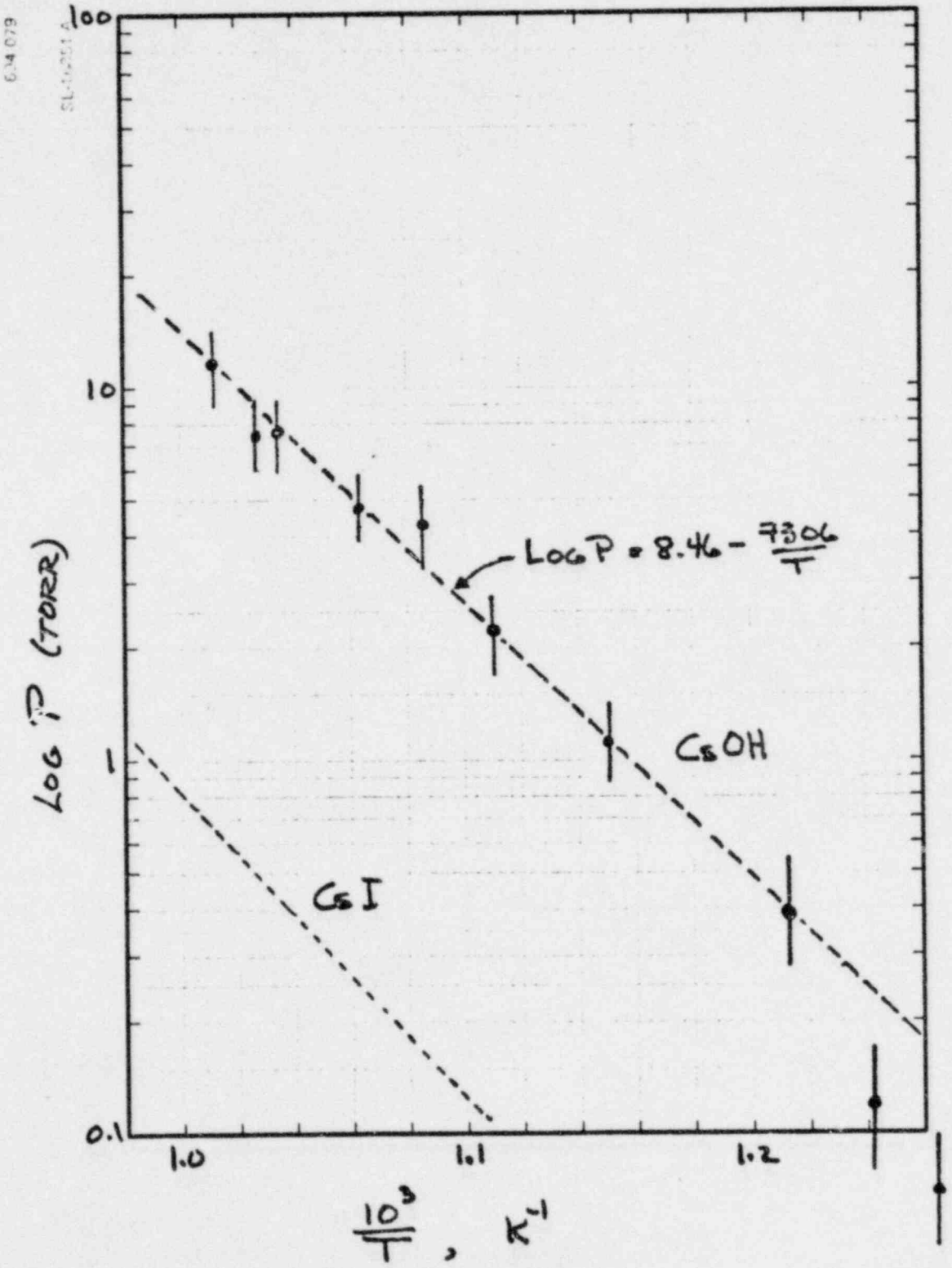

FIGURE 1

H_2 ROTATIONAL RAMAN SPECTRA -- INTERIM CELL

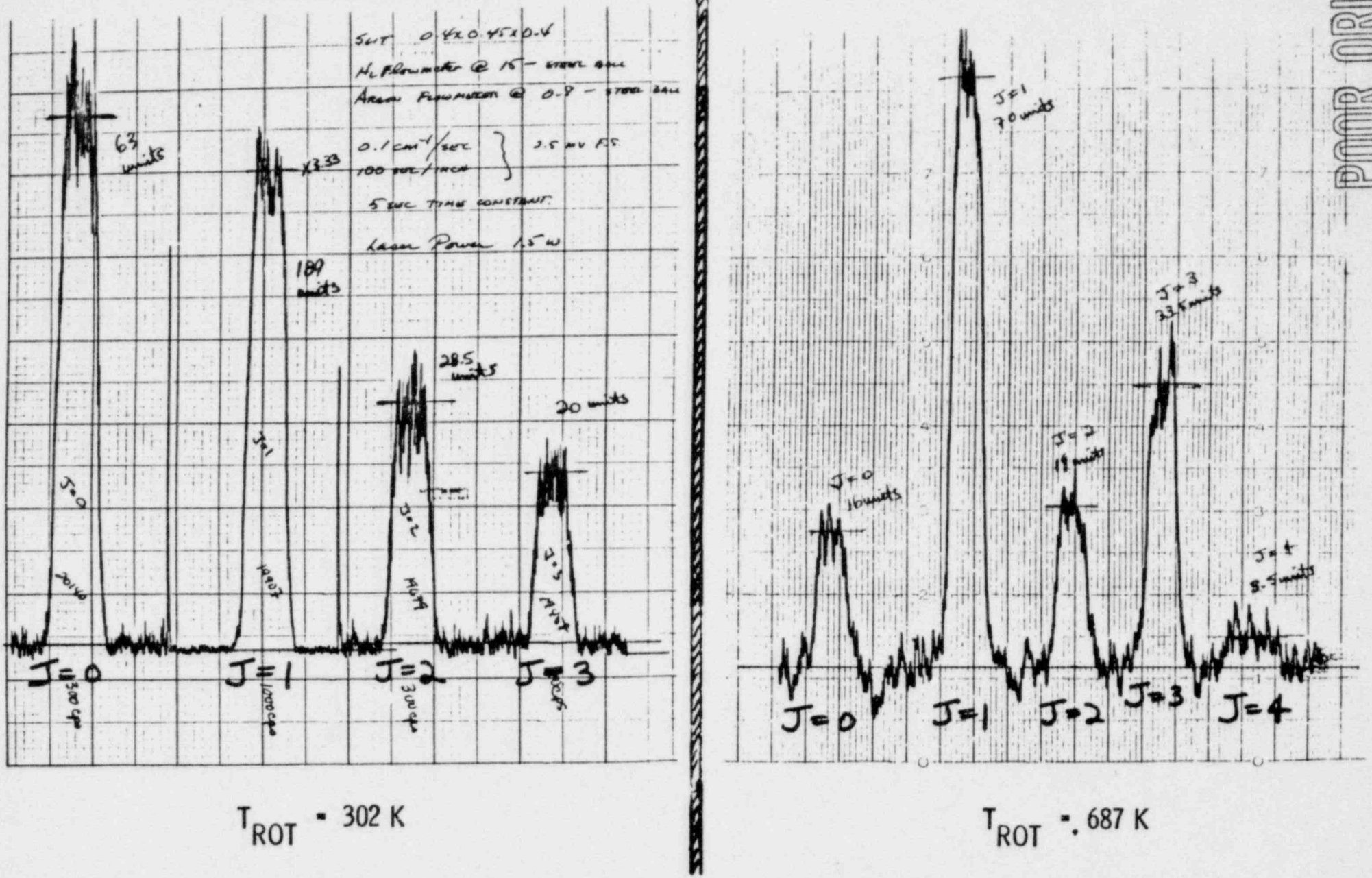

FIGURE 2

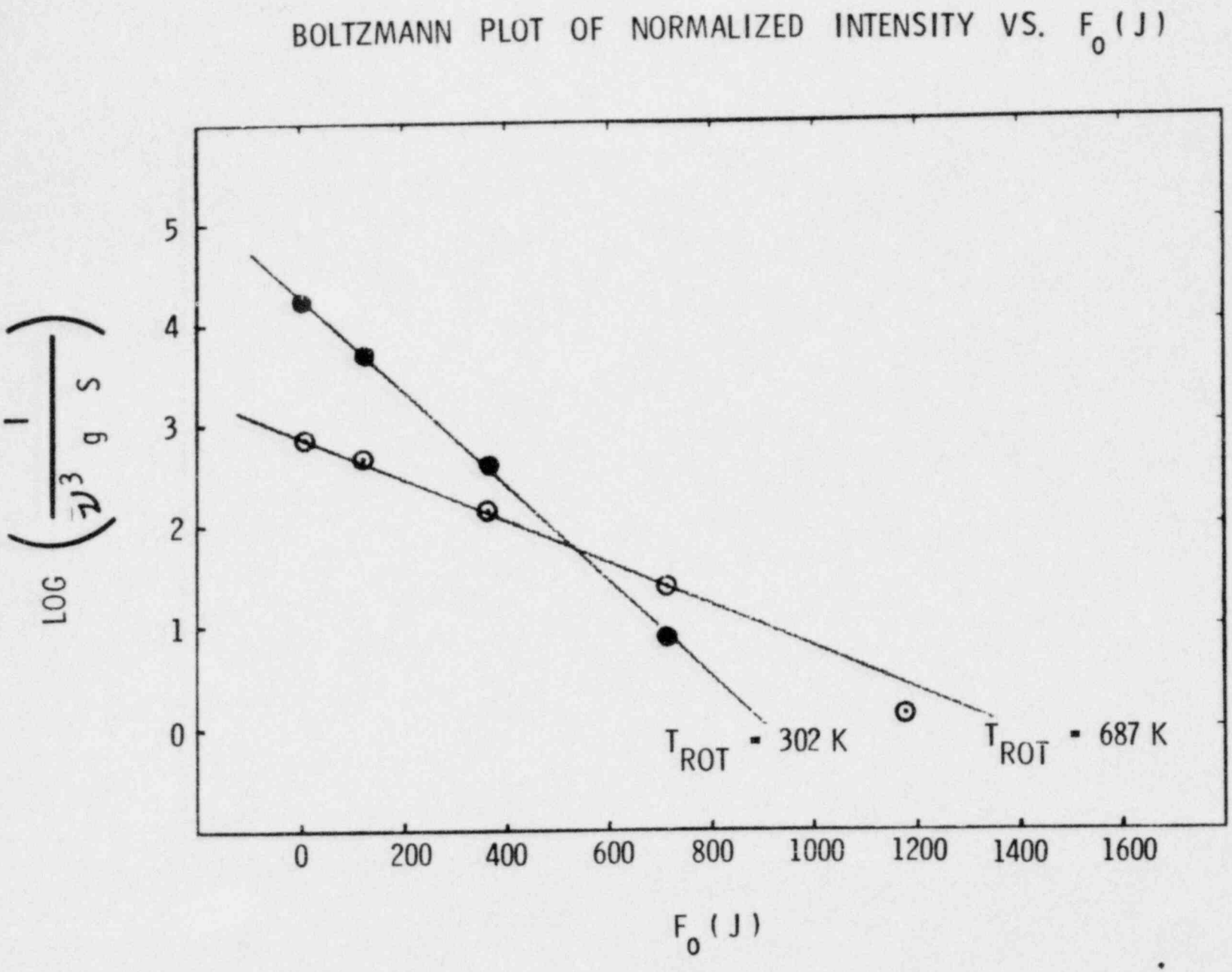
BOLTZMANN PLOT OF NORMALIZED INTENSITY VS. $F_0(J)$
$\log\left(\frac{I}{\bar{\nu}^3 g S}\right)$
5
4
3
2
1
0
0
200
400
600
800
1000
1200
1400
1600
$F_0(J)$
T_{ROT} = 302 K
T_{ROT} = 687 K

FIGURE 3